J Mater Sci (2007) 42:6672–6683
DOI 10.1007/s10853-007-1522-0

# Homogeneous and heterogeneous melting behavior of bulk and nanometer-sized Cu systems: a numerical study

**G. Manai · F. Delogu**

Received: 17 July 2006 / Accepted: 16 January 2007 / Published online: 1 May 2007


**Abstract** Molecular dynamics simulations have been used to investigate the solid–liquid transition of different Cu systems. These consisted of surface-free crystalline bulks and semi-crystals terminating with a free surface as well as of particles and wires with different shape and size in the mesoscale regime. The characteristic melting points of the various systems were attained by gradual heating starting from 300 K. Apart from surface-free bulk systems, where the phase transition at the limit of superheating is homogeneous, melting displays heterogeneous character. This is due to the existence of surface layers with structural and energetic properties different from the ones of bulk-like interior. Simulations point out a significant depression of both the melting point and latent heat of fusion for nanometer-sized systems respect to semi-crystals. Below the characteristic melting point, free surfaces are involved in pre-melting processes determining the formation of a solid–liquid interface. The onset of melting is related to the formation of a critical amount of lattice defects and this provides a common basis for the rationalization of homogeneous and heterogeneous melting processes despite their intrinsic differences.

## Introduction

It is well known that the physical and chemical properties of systems in the mesoscale regime between atomic clusters and bulk systems undergo smooth variations, which can be described by relatively simple power laws depending on the system size [1–4]. A typical example is represented by the depression of the melting point as the system size decreases, theoretically predicted for small metallic particles in 1909 [5] and experimentally observed decades later [6–9]. Even though the observations can receive a phenomenological explanation with the size dependence of the chemical potential of atoms and molecules in finite systems [5, 10–15], the knowledge of atomic-scale processes underlying such behavior is still unsatisfactory. In other words, a conceptual framework able to rationalize the whole thermodynamic behavior is lacking [16–19].

A deeper insight into the atomic-scale mechanisms governing the occurrence of melting can be obtained by comparing the transition behavior of bulk and nanometer-sized systems with the aim of pointing out unexpected relationships between them [20]. The solid–liquid phase transformation transition can take place with either homogeneous or heterogeneous features depending on the suppression of surface effects [21–29]. As a consequence of the successful connection between melting and structural defects established for two-dimensional systems by the so-called KTHNY theory [31–32], dislocation-mediated melting mechanisms are currently regarded as promising candidates for rationalizing three-dimensional melting processes [20, 22, 33–35].

The present work aims at comparing the melting behavior of bulk systems with and without a free surface with the one of particles and wires of different shape and size. The study focuses in particular on lattice distortions and defects, identified and enumerated by means of molecular dynamics simulations. The methodologies employed in calculations largely exploit the existing literature

G. Manai
Department of Physics, Trinity College, Dublin 2, Ireland

F. Delogu (✉)
Dipartimento di Ingegneria Chimica e Materiali, Università degli Studi di Cagliari, piazza d'Armi, 09123 Cagliari, Italy
e-mail: delogu@dicm.unica.it

[20, 22, 26, 34–44] and are briefly described in the following.

## Molecular dynamics simulations

Computations were carried out on Cu systems. Interactions between Cu atoms were described by a semi-empirical tight-binding (TB) potential based on the second-moment approximation to the electronic density of states [45–47]. The cohesive energy was then expressed as

$$E = \sum_{i=1}^{N} \left\{ \sum_{j=1}^{N} A e^{-p\left(\frac{r_{ij}}{r_0}-1\right)} - \left[ \sum_{j=1}^{N} \xi^2 e^{-2q\left(\frac{r_{ij}}{r_0}-1\right)} \right]^{\frac{1}{2}} \right\}, \quad (1)$$

where $r_0$ is the nearest-neighbors distance at 0 K and $r_{ij} = |r_i - r_j|$ the distance between atoms $i$ and $j$. The characteristic values of the potential parameters $A$, $\xi$, $p$ and $q$ were taken from the literature [47]. Forces were computed within a cutoff distance including the seventh shell of neighbors. Both thermodynamic and elastic properties of Cu bulk systems are thus satisfactorily reproduced. For example, the enthalpy of vacancy formation obtained, amounting to about 350 kJ mol$^{-1}$, compares remarkably well with the experimental range of values between about 164 and 415 kJ mol$^{-1}$ [48]. The thermal expansion coefficient was found to be roughly equal to $1.95 \times 10^{-5}$ K$^{-1}$, a value remarkably close to the experimental one of about $2.1 \times 10^{-5}$ K$^{-1}$ [49]. According to literature, experimental values of elastic constants are reproduced up to 1% [47].

Though capable of describing remarkably well bulk atomic interactions [45–47], the TB potential is not particularly suited for simulating surface properties, which are instead better reproduced by the Finnis–Sinclair force scheme [50] and the embedded-atom-method [51]. The TB potential permits however accurate simulations of both face-centered-cubic (fcc) and hexagonal-close-packed (hcp) metallic structures [45–47]. It represents then a natural choice for studying fcc metals despite the drawbacks in the estimation of surface properties, also in the light of the fact that the present study is aimed to study the Cu melting behavior exclusively on a qualitative basis.

Calculations were carried out within the isobaric-isothermal Nosè–Andersen (*NPT*) ensemble with number of atoms $N$, temperature $T$ and pressure $P$ constant [52, 53]. The Parrinello–Rahman scheme was also implemented to properly deal with eventual changes in the crystallographic cell shape [54]. The equations of motion were solved by applying a fifth-order predictor-corrector algorithm [55] with a time step $\delta t$ equal to 2.0 fs.

The long-range structural order within the different bulk systems was investigated by means of the conventional two- and three-dimensional static order parameters $S_p(\boldsymbol{k})$ and $S(\boldsymbol{k})$ [26, 39, 40, 55]. The latter is defined as

$$S(\boldsymbol{k}) = \frac{1}{N} \left\{ \left[ \sum_{i=1}^{N} \cos(\boldsymbol{k} \cdot \boldsymbol{r}_i) \right]^2 + \left[ \sum_{i=1}^{N} \sin(\boldsymbol{k} \cdot \boldsymbol{r}_i) \right]^2 \right\}^{\frac{1}{2}} \quad (2)$$

where the wave vector $\boldsymbol{k}$ is a reciprocal lattice plane vector and $\boldsymbol{r}_i$ is the vector defining the position of the $i$th atom in the atomic plane. $N$ is the total number of atoms. For an ideal crystal at 0 K, $S(\boldsymbol{k})$ equals unity for any wave vector $\boldsymbol{k}$. By contrast, in a completely disordered configuration $S(\boldsymbol{k})$ fluctuates near zero. $S(\boldsymbol{k})$ provides thus a direct quantitative measure of the degree of structural disorder in the system. The degree of disorder was evaluated by using the crystallographic vectors [111] and [100] and the relative $S(\boldsymbol{k})$ averaged at each time step. When appropriate, a similar method was employed to evaluate plane-by-plane the $S_p(\boldsymbol{k})$ values. Disorder was also monitored by means of the pair correlation function (PCF) [55]. The relationship between potential energy $U$ and structural order was exploited to follow the gradual thermal disordering and the final collapse of the crystalline lattice [36, 39, 40, 43, 44].

Local crystalline order was quantified by means of the Honeycutt–Andersen (HA) parameters [38], which also permit the identification of stacking faults. Local lattice distortions and defects were characterized by identifying the atoms with defective coordination, i.e. with a number of nearest neighbors different from 12. The number of nearest neighbors was evaluated at each simulation step for each atom by applying a distance criterion. Accordingly, two atoms were regarded as nearest neighbors when located at distances shorter than the one, $r_{min}$, corresponding to the first minimum of the PCF [34, 35]. Any atom with defective coordination will be hereafter referred to as defective. The formation of point and extended lattice defects such as vacancies, interstitials and dislocations was pointed out by analyzing the spatial correlation between defective atoms. The number $N_{cl}$ and size $n$ of their aggregates, or clusters, were identified and classified by using the same aforementioned distance criterion [34, 35]. Two defective atoms were thus regarded as belonging to the same aggregate when located at distances shorter than $r_{min}$. Direct visualization technique based on the color coding of atomic species depending on their coordination number were also used to identify lattice defects [56].

## Homogeneous melting of a surface-free bulk system

The homogeneous nucleation of melting in a perfect crystalline bulk establishes the maximum limit of super-

heating $T_m^k$ [23, 24]. Contrary to what happens in experiments, $T_m^k$ can be easily attained in numerical simulations studying the behavior of defect- and surface-free crystalline bulks. Surface effects are indeed completely eliminated by imposing periodic boundary conditions (PBCs) along the three Cartesian directions [55].

Molecular dynamics (MD) simulations were essentially performed on a system of 6,912 atoms arranged in the fcc *cF*4 lattice. Smaller systems containing 500, 2,048 and 4,000 were also used to point out possible size effects. In any case, the initial configuration was relaxed at 300 K and roughly null external pressure for 200 ps. The system was then gradually heated by raising the temperature of 25 K every 20 ps, corresponding to a nominal heating rate of 1.25 K $ps^{-1}$. Nominal heating rates of 0.5, 1 and 2 K $ps^{-1}$, obtained by keeping the relaxation interval 20 ps long, were also explored to ascertain possible heating rate effects on the homogeneous melting point $T_m^k$.

Let us consider first the case of the system containing 6,912 atoms and heated at a rate of 1.25 K $ps^{-1}$. As expected, heating is accompanied by a gradual increase of thermal disorder. Correspondingly, the static order parameter $S(\boldsymbol{k})$ undergoes a progressive decrease culminating in a sudden downward drop. Such decrease marks the failure of the crystalline lattice and identifies the limit of superheating $T_m^k$, amounting to about 1,650 K [26, 39, 40]. The estimate of homogeneous melting point $T_m^k$ is affected by size effects. These become evident when the limit of superheating $T_m^k$ obtained for different bulk systems is reported as a function of their size. The data quoted in Fig. 1 indicate that $T_m^k$ increases with the total number of atoms. It is worth noting that the limit of superheating $T_m^k$ for the system of 6,912 atoms is also affected by the rate at which temperature is raised. Figure 2 shows indeed that $T_m^k$ decreases as the nominal heating rate increases as a result

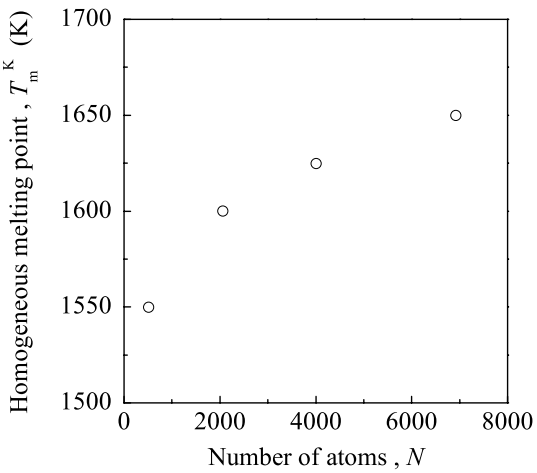


**Fig. 1** The increase of the homogeneous melting point $T_m^k$ with the number of atoms $N$, which quantifies the system size

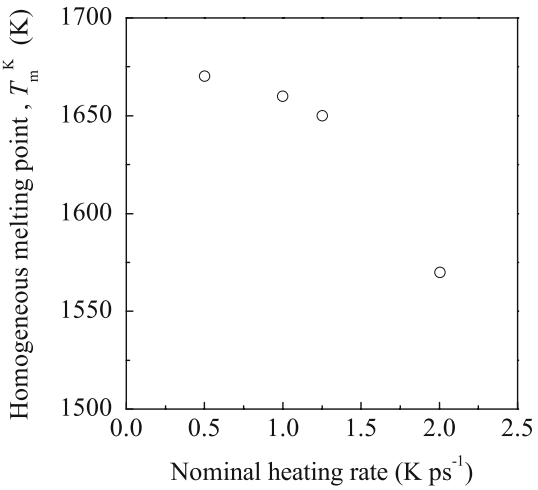


**Fig. 2** The change of the homogeneous melting point $T_m^k$ with the nominal heating rate

of the increasing difficulty of accommodating local atomic strains. For sake of clarity, it must be noted that in the different cases the homogeneous melting point $T_m^k$ was identified with the temperature at which $S(\boldsymbol{k})$ took values smaller than 0.7. Such behavior will be hereafter considered as a simplified melting criterion. Correspondingly, the solid–liquid transition occurs by definition at the temperature at which $S(\boldsymbol{k})$ becomes smaller than 0.7.

The progressive thermal disordering of the crystalline lattice is accompanied by the appearance of pairs of defective atoms. Defective atoms are generally 11- and 13-fold coordinated, whereas other defective coordination numbers are rarely observed. Their generation is related to the rearrangement of the coordination shells of two neighboring atoms due to the increase of their thermal

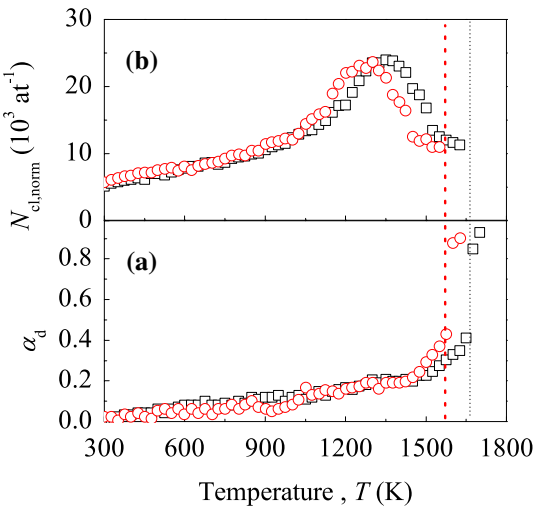


**Fig. 3** The fraction $\alpha_d$ of defective atoms (**a**) and the normalized number $N_{cl,norm}$ of clusters of defective atoms (**b**) as a function of the temperature $T$ for the systems with 500 (○) and 6912 (□) atoms

vibration amplitudes and the consequent increase of their reciprocal hindrance. As shown in Fig. 3a, their fraction $\alpha_d$, corresponding to the ratio between the number of defective atoms and the total number of atoms in the system, increases with the temperature $T$ according to a non-linear trend. In accordance with previous studies on different systems [34, 35], at $T_m^k$ the fraction $\alpha_d$ amounts approximately to 0.4. This scenario is reminiscent of the one proposed by the KTHNY theory for two-dimensional systems [20, 22, 30–32, 58–61], where thermal disorder induces first the formation of dislocation quadrupoles and then their disassociation.

The cooperative character of the defective atom generation process at relatively high temperatures, which determines the appearance of defective atom pairs in the neighborhood of pre-existing ones [60, 61], finally results in the formation of defective atom clusters. The number $N_{cl}$ of such structures changes with the temperature according to the curve shown in Fig. 3b. For sake of comparison, the $N_{cl}$ data have been however normalized to the total number of atoms of the system considered, i.e. 6,912. The smooth non-linear trend has a maximum at 1,325 K, which originates from the competition between ramification, fragmentation and coalescence events [62, 63].

Defective atom clusters can be occasionally identified with dislocations and point defects. This is the case of aggregates of twelve 11-fold coordinated atoms, which correspond to individual vacancies, and of twelve 13-fold coordinated atoms, corresponding to individual interstitials. Shockley partial dislocations with a (111) glide plane and moving irregularly in the [110] and one of the [211] crystallographic directions can be also identified by means of direct visualization. A couple of Shockley partial dislocation loops is shown in Fig. 4. Such loops point out the formation of stacking faults enclosing crystalline domains of about 30–40 atoms with a hcp arrangement. Open dislocation lines with a (111) glide plane are observed only at temperatures close to the homogeneous melting point.

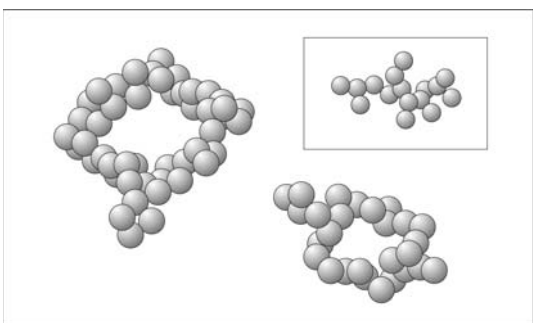

**Fig. 4** A pair of Shockley partial dislocation loops. A cluster of defective atoms is also shown in the inset. The snapshot refers to the system containing 6912 atoms

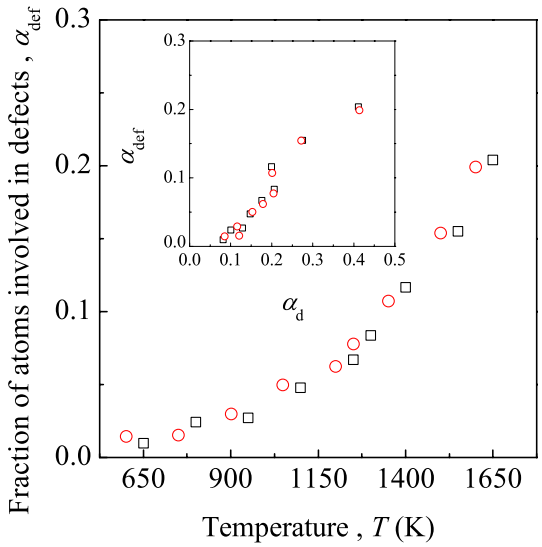


**Fig. 5** The fraction $\alpha_{def}$ of atoms involved in lattice defects as a function of the temperature $T$. The relationship between $\alpha_{def}$ and the fraction $\alpha_d$ of defective atoms is shown in the inset. Data pertain to the systems with 4000 (○) and 6912 (□) atoms

The fraction $\alpha_{def}$ of defective atoms involved in lattice defects can be roughly estimated only at temperatures above 800 K, being too much lower below. Its change with the temperature is shown in Fig. 5. At $T_m^k$, $\alpha_{def}$ amounts approximately to 0.2.

## Heterogeneous melting of a semi-crystal

The temperature $T_{m,0}$ at which the heterogeneous melting process takes place is identified by the equality of the Gibbs free energies of solid and liquid phases [20–22]. When present, melting initiates at surfaces, interfaces and other structural heterogeneities [20–22, 36, 37, 60]. The present work analyzes the heterogeneous melting processes occurring on plane surfaces with different topology. The transition is simulated by exploiting a previously developed methodology [40]. The undamped collective motion of the surface atomic layers is avoided by preparing the system from a configuration of atoms arranged in a stacking sequence of 58 atomic planes [41]. In order to study the effect of the surface topology on the heterogeneous melting process the planes with Miller indexes (100), (110) and (111) were used. The systems consisted in all the cases of 8,352 atoms. PBCs were applied only along the $x$ and $y$ Cartesian directions, whereas two reservoir regions of five atomic planes each containing immobile atoms with a perfect fcc arrangement were defined along the $z$ Cartesian direction. The system was equilibrated for 20 ps at 300 K and roughly null external pressure. The simulation cell was divided into two regions referred to as $C$ and $D$

and extending, respectively, from the 1st to 48th atomic planes and from the 49th to 58th ones. A relaxed free surface was created by canceling the pair interactions between $C$ and $D$ atoms by linearly decreasing to zero the potential parameters $A$ and $\xi$ in 2 ps. A further relaxation 200 ps long was carried out. The heterogeneous solid–liquid transition was therefore simulated on systems of 6,912 atoms arranged in 48 (100), (110) and (111) atomic planes terminating with a free surface and a reservoir region on the opposite sides. To properly deal with the gradual thermal expansion due to the temperature rise, the reservoir was artificially expanded by rescaling at each temperature rise the position of its atoms in order to equalize the reservoir elementary cell parameter to the bulk one at the same temperature. An empty space about ten atomic planes high, bounded by a reflective barrier, was defined at the top of the simulation cell to permit surface atoms to pass from the solid to the vapor phase. A schematic of the system is reported in Fig. 6.

The comparison between the planar static order parameter $S_p(\boldsymbol{k})$ values for the systems here investigated and for similar systems enclosed by PBCs points out the existence of a certain ordering in the mobile planes adjacent the ordered immobile reservoir. Such ordering decreases rapidly with the distance from the reservoir and the temperature, disappearing on the average already at the 11th or 12th plane. It therefore does not affect the surface dynamics. Surface effects are confined to a thin layer the thickness $\Delta$ of which amounts approximately to three

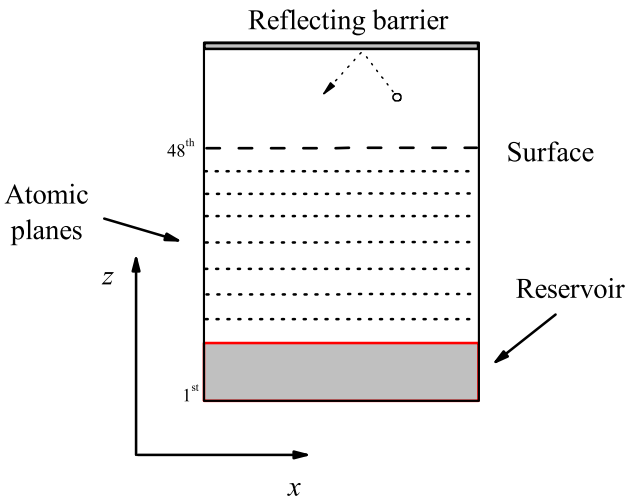


**Fig. 6** A schematic illustration of the simulation box. The system consists of a stacking of 48 (110) atomic planes along the Cartesian $z$ direction. At the top it terminates with a free surface. An empty space is left to permit the evaporation of atomic species at the free surface. The free space is closed by a reflecting barrier to keep constant the total number of atoms in the system. The reservoir region at the bottom contains instead immobile atomic species arranged on a perfect fcc lattice

atomic planes, i.e. about 0.5 nm, at 300 K. Such planes possess indeed an average potential energy $U$ deviating from the value $U_{bulk}$ characteristic of a surface-free bulk at the same temperature and pressure. In addition, the $S_p(\boldsymbol{k})$ values of the 46th, 47th and 48th planes are significantly lower than the $S_p(\boldsymbol{k})$ values of bulk planes. It follows that the planes below the 46th one can be regarded as bulk-like planes.

Surface planes are significantly more disordered than bulk ones at each given temperature as a consequence of the higher mobility of surface atoms. These undergo displacements of various length and form so-called vacancy-adatom pairs [40, 41]. Vacancies initially localized at surface can successively migrate towards the bulk *via* local rearrangements of atomic configurations. In all the systems, at a certain temperature the $S(\boldsymbol{k})$ value of the crystalline region including the 46th, 47th and 48th planes becomes smaller than 0.7 and the dynamics of atomic species at surface displays liquid-like features exemplified by the trajectories quoted in Fig. 6. Surface planes are then affected by pre-melting phenomena. Pre-melting points $T_{pm,0}$ depend on the topology of the crystallographic plane at the free surface. In particular, data quoted in Table 1 indicate that $T_{pm,0}$ increases as the surface atomic packing increases. This means that, as observed in previous work [60], loose-packed surfaces melt first.

The solid–liquid interface nucleated at $T_{pm,0}$ and involving the three surface planes is stable up to a temperature $T_{m,0}$, temperature above which the $S(\boldsymbol{k})$ value of the crystalline region including the 45th, 44th and 43rd planes becomes smaller than 0.7. The solid–liquid interface propagates then into the bulk region at rates on the order of 20 m $s^{-1}$. The temperature $T_{m,0}$ can be thus regarded as the equilibrium melting point, dependent on potential and methodologies employed [39,40], of the bulk system with a plane free surface. Contrary to $T_{pm,0}$ values, as evident from Table 1 the melting point $T_{m,0}$ is only slightly dependent on the topology of the crystallographic planes. The latent heats of fusion $\Delta H_{m,0}$, given by the difference between the average potential energies $U$ of the liquid and solid phases, respectively, are also quoted in Table 1. It can be seen that both $T_{m,0}$ and $\Delta H_{m,0}$ are smaller than the experimental values of 1,357 and 13.02 kJ $mol^{-1}$,

**Table 1** The pre-melting point $T_{pm,0}$, the melting point $T_{m,0}$ and the latent heat of fusion $\Delta H_{m,0}$ for the systems consisting of 6,912 atoms and terminating with (100), (110) and (111) free surfaces

| | (100) | (110) | (111) |
|---|---|---|---|
| $T_{pm,0}$ (K) | 1,175 | 1,200 | 1,225 |
| $T_{m,0}$ (K) | 1,275 | 1,275 | 1,300 |
| $\Delta H_{m,0}$ (kJ $mol^{-1}$) | 12.92 | 12.83 | 12.98 |

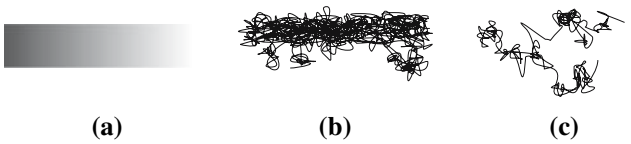


**Fig. 7** (**a**) A schematic representation of the semi-crystal structure. A central section of the surface layer in light gray about 0.5 nm thick. (**b**) A portion of the trajectories followed by the atomic species located approximately in the central slice at 1250 K. (**c**) The two-dimensional projection of the three-dimensional trajectory followed at 1250 K by an atom belonging to the surface layer

respectively [49]. Such behavior can be mostly ascribed to the high heating rate. As shown in Fig. 7 this latter significantly affects the pre-melting, $T_{pm,0}$, and melting, $T_{m,0}$, point values. Such temperatures increase indeed as the heating rate decreases.

It should be also noted that the pre-melting and melting temperatures as well as the latent heat of fusion are a function of the system size. The accuracy of the estimates significantly increases indeed as the system size increases. No systematic investigation was here performed with regard to this point. However, the pre-melting point $T_{pm,0}$ and the melting temperature $T_{m,0}$ were found to amount approximately to 1,284 and 1,326 K, respectively, for a system of about 20,000 Cu atoms arranged in a stacking of 48 (110) planes terminating with a free surface and a reservoir on opposite sides along the $z$ Cartesian direction. The latent heat of fusion $\Delta H_{m,0}$ was approximately equal to 12.9 kJ mol$^{-1}$. Heating was carried out in this case at 2 K every 20 ps of relaxation.

The atomistic details of the heterogeneous transition were analyzed by dividing the bulk into 11 slices consisting of three atomic planes each. However, the atomic planes affected by reservoir-induced ordering and surface-induced pre-melting phenomena were not included. The first slice considered includes then the 13th, 14th and 15th planes and the last one the 43rd, 44th and 45th planes. To a large extent vacancies appear in the bulk region as a consequence of migration processes from the surface, being the formation of vacancy-interstitial complexes quite rare. At the same time, defective atoms also appear. Their generation was followed by evaluating the fraction $\alpha_{d,s}$ of defective atoms in each slice s, defined as the ratio between the number of defective atoms and the total number of atoms in the slice. The $\alpha_{d,s}$ values at the equilibrium melting point $T_{m,0}$ are quoted in Fig. 8a as a function of the slice number s. A non-uniform distribution of defective atoms is observed, with the $\alpha_{d,s}$ values decreasing smoothly along the $z$ Cartesian direction as the distance from the free surface increases. As shown in Fig. 8b, the static order parameter $S(\boldsymbol{k})$ values for each slice s strictly parallel the trend of the $\alpha_{d,s}$ values. It is worth noting that at $T_{m,0}$ only the 11th slice has $S(\boldsymbol{k})$ below 0.7 and is therefore melting.

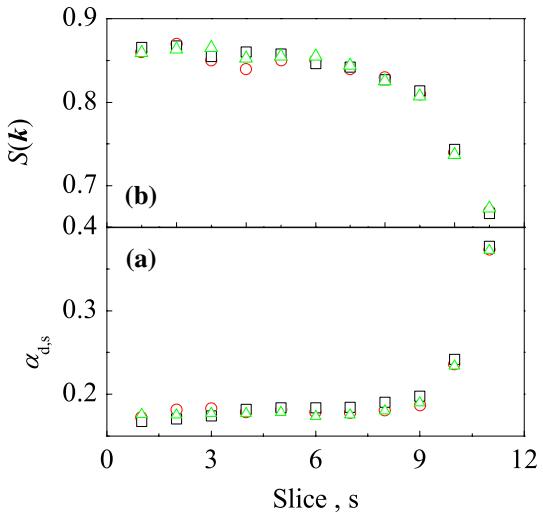


**Fig. 8** The fraction $\alpha_{d,s}$ of defective atoms (**a**) and the static order parameter $S(\boldsymbol{k})$ (**b**) for the s slices at the equilibrium melting point $T_{m,0}$. The $\alpha_{d,s}$ values arrange along the $z$ Cartesian direction according to an increasing trend and the 11th slice, the one immediately below the surface layer, is characterized by a fraction $\alpha_{d,11}$ of defective atoms equal to about 0.37. In accordance with $\alpha_{d,s}$ data, $S(\boldsymbol{k})$ decreases as the surface is approached, pointing out an increase of structural disorder. Data pertain to the systems with (100) (△), (110) (○) and (111) (□) atomic plane stacking

The fraction $\alpha_{d,11}$ of defective atoms in the 11th slice at $T_{m,0}$, amounting to about 0.37, is then very close to the one observed in the surface-free bulk at the limit of superheating $T_m^k$. Figure 8a clearly indicates that this is true for all the systems investigated irrespective of the atomic plane topology. Further analyses point out that, on the average, the fraction $\alpha_{d,s}$ of defective atoms in a given slice s immediately after its $S(\boldsymbol{k})$ value has gone below 0.7 amounts to 0.38 ± 0.04.

The formation of a molten layer at the free surface at temperatures above $T_{pm,0}$ greatly affects the distribution of defective atoms in the system as well as the shape and number of defective atom clusters. The profile of $\alpha_{d,s}$ values reported in Fig. 8a clearly indicates that the concentration of defective atoms is larger in the region below the solid–liquid interface. Correspondingly, defective atoms form clusters with the main body located immediately below the propagating solid–liquid interface. The cluster depicted in Fig. 9 for sake of illustration points out in addition the existence of filamentary aggregates that, extending below the main cluster body, play an important role in the solid–liquid interface propagation. Such columnar arrangements can be indeed regarded as preferred nucleation sites for the appearance of further defective atoms.

The preferential clustering of defective atoms in the region below the solid–liquid interface favors the occurrence of cluster coalescence events. As a consequence, the

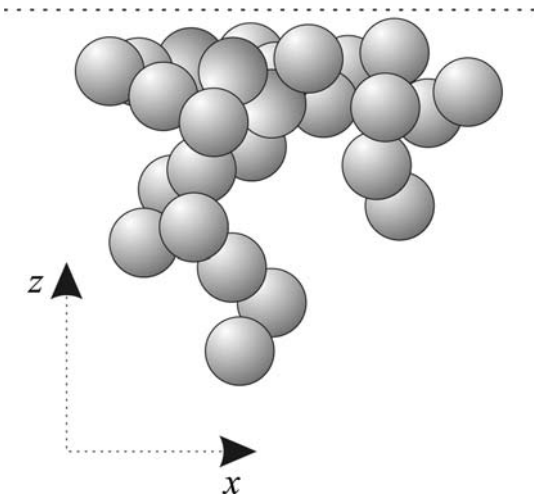


**Fig. 9** A cluster of defective atoms lying below the solid–liquid interface, whose average position is marked by the horizontal dotted line

total number of clusters is expected to be smaller than in the surface-free bulk at the same temperature. The normalized number $N_{cl,norm}$ of defective atom clusters quoted in Fig. 10 as a function of the temperature $T$ demonstrates that this is actually the case. The data refer to the bulk region between the 13th and the 46th planes and are normalized to 4,752 atoms. In analogy with the case of the surface-free bulk, a certain number of defective atoms can be identified with Shockley partial dislocations with a (111) glide plane, moving irregularly in the [110] and one

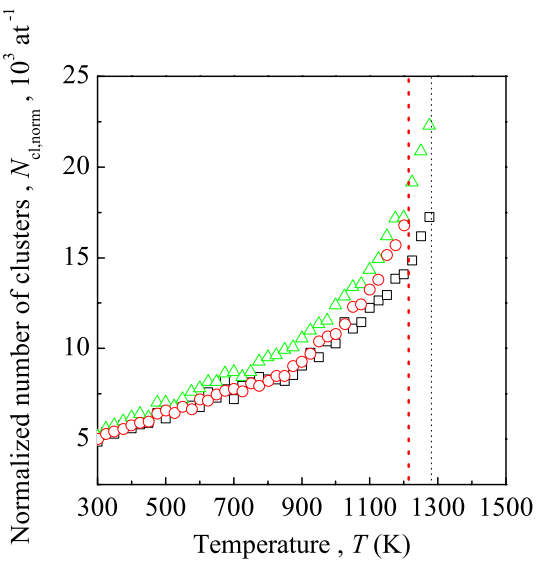


**Fig. 10** The normalized number $N_{cl,norm}$ of clusters of defective atoms as a function of the temperature $T$. $N_{cl,norm}$ undergoes a monotonic increase up to the equilibrium melting point $T_{m,0}$. Data pertain to the systems with (100) (△), (110) (○) and (111) (□) atomic plane stacking

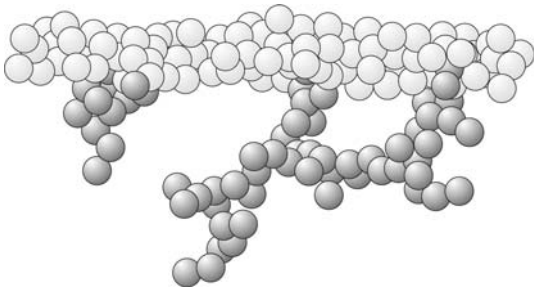

**Fig. 11** An open dislocation (right) and a cluster of defective atoms (left) at the free surface. Molten phase atoms are indicated light gray

of the [211] crystallographic directions. Crystalline domains of about 30–40 atoms with a hcp arrangement are also observed. Different from the previous case, the presence of either the free surface or of the molten layer permits however the formation of open dislocations such as the one depicted in Fig. 11. The fraction $\alpha_{def,s}$ of defective atoms involved in lattice defects in each given slice s undergoing melting roughly amounts on the average to $0.2 \pm 0.04$. As in the case of the $\alpha_{d,s}$ values, the $\alpha_{def,s}$ values at melting are thus close to the ones already observed when the surface-free bulk undergoes the homogeneous melting at the limit of superheating $T_m^k$.

## Heterogeneous melting of nanometer-sized spherical particles

Due to their free surface, unsupported particles undergo heterogeneous melting processes analogous in principle to the one of semi-crystals discussed above. Their melting points $T_m$ are however significantly depressed respect to the equilibrium melting point $T_{m,0}$ of a bulk system [5–19, 43, 44]. The present section will focus on the melting behavior of spherical particles with radius of about 4 and 8 nm. Full details of the simulation procedure briefly described below can be found elsewhere [44].

A system of 562,432 atoms, arranged in $52 \times 52 \times 52$ fcc elementary cells and enclosed by PBCs along the three Cartesian directions, was relaxed in the (*NPT*) ensemble at 300 K and roughly null external pressure for 100 ps. The relaxed configuration obtained will be hereafter referred to as the parent configuration, given that any nanometer-sized system will be prepared starting from it. The particles with radius equal to about 4 and 8 nm were prepared by selecting out two spherical portions and gradually canceling the interactions between the atoms within the sphere and the ones outside. Cancellation was performed according to a linear decrease to zero in 1.6 ps the potential parameters $A$ and $\xi$ for the aforementioned pair interactions. The relaxed particles consisted of 22,303 and 203,854 atoms, respectively. Simulations were then per-

formed within the (*NhT*) ensemble with number of atoms *N*, shape *h* and temperature *T* constant. The temperature was raised of 10 K every 40 ps, i.e. at a nominal rate of 0.25 K $ps^{-1}$.

The nanometer-sized particles consist of a disordered surface layer and an ordered crystalline interior [44]. Average atomic positions in the bulk-like particle interior, defined by the atomic trajectories within a time interval of 2 ps, were used to define the crystallographic vectors describing the fcc lattice. Theoretically expected positions were thus worked out in order to quantify the structural disorder by comparing the real atomic positions with the theoretically expected ones [44]. This permitted to employ again the static order parameter $S(\boldsymbol{k})$ to measure the degree of structural order within the four and eight spherical shells about 1 nm thick into which the interior of the 4 and 8 nm particles was divided. The fourth and eighth surface shells, respectively, of the 4 and 8 nm particles are characterized by $S(\boldsymbol{k})$ values close to 0.7 even at relatively low temperature and are involved in pre-melting phenomena approximately at 1,050 and 1,120 K, as also evident from the atomic trajectories shown in Fig. 12.

The solid–liquid interface of the 4 and 8 nm particles is stable up to 1,180 and 1,220 K, respectively. Above such values, the $S(\boldsymbol{k})$ values of the third shell of the 4 nm particle and of the seventh shell of the 8 nm particle become smaller than 0.7 and the interface starts its propagation progressively involving all the bulk-like region. Such process takes place at rates on the order of 100 m $s^{-1}$ for

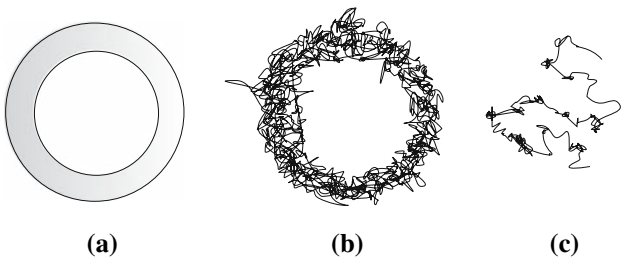


**Fig. 12** (**a**) A schematic representation of the two-state structure of the 4 nm particle. The surface layer is in light gray. (**b**) A portion of the trajectories followed by the atomic species at 1100 K for a central slice of the particle having a thickness of 0.5 nm. (**c**) The two-dimensional projection of the three-dimensional trajectory followed at 1100 K by an atom belonging to the surface layer

**Table 2** The pre-melting point $T_{pm}$, the melting point $T_m$ and the latent heat of fusion $\Delta H_m$ for the 4 and 8 nm spherical particles [44]

| | 4 nm | 8 nm |
|---|---|---|
| $T_{pm,0}$ (K) | 1,050 | 1,120 |
| $T_m$ (K) | 1,180 | 1,220 |
| $\Delta H_m$ (kJ $mol^{-1}$) | 10.66 | 11.78 |

temperatures about 50 K above the melting point $T_m$. The thermal properties of the particles are reported in Table 2.

The radial profiles of the fraction $\alpha_{d,s}$ of defective atoms in the various shells at the melting point $T_m$ are reported in Fig. 13a and b for the 4 and 8 nm particles, respectively. As already observed in the case of systems with a free plane surface, the fraction $\alpha_{d,s}$ of atoms with defective coordination located within each given shell s decreases smoothly with the distance from the free surface. In particular, both the fractions $\alpha_{d,3}$ and $\alpha_{d,7}$ of defective atoms in the third and seventh shells amount approximately to 0.37, a value close to the ones observed in bulk solids at $T_m^k$ and in the melting slices below either a free surface or a solid–liquid interface at $T_{m,0}$. On the average, a given spherical shell s undergoes melting when the fraction $\alpha_{d,s}$ of defective atoms it contains amounts to 0.39 ± 0.03.

Also in the case of spherical particles, defective atoms form clusters of different size and shape. The normalized number $N_{cl,norm}$ of such aggregates is quoted as a function of the temperature *T* in Fig. 14 for the case of the 4 nm particle. It can be seen that at any given temperature these $N_{cl,norm}$ values are significantly smaller than the ones observed in a surface-free bulk and in a semi-crystal. Similar results are obtained for the 8 nm particle. The comparison between the data sets in Figs. 3b, 10 and 13 clearly points out that the occurrence of cluster coalescence events is more favored in the particle rather than in the bulk systems considered. This is a consequence of the system geometry, which in turn affects the shape of the clusters lying below the surface layer. Figure 15 shows that the main body of the clusters is located immediately below the solid–liquid

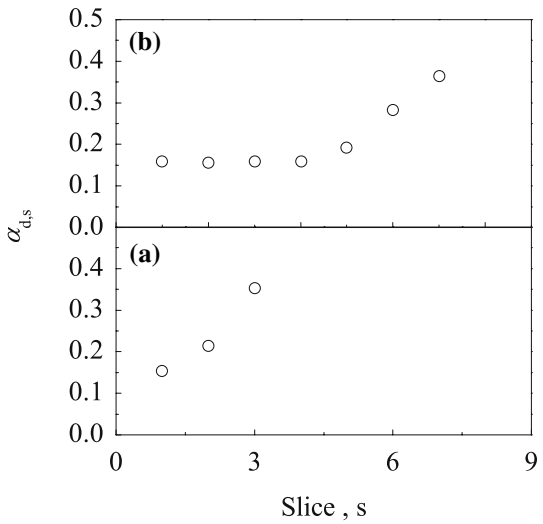


**Fig. 13** The fraction $\alpha_{d,s}$ of defective atoms for the s slices at the equilibrium melting point $T_m$. The $\alpha_{d,s}$ values refer to the (**a**) 4 nm and (**b**) 8 nm particles. In both cases the slice immediately below the surface layer is characterized by a fraction of defective atoms equal to about 0.37

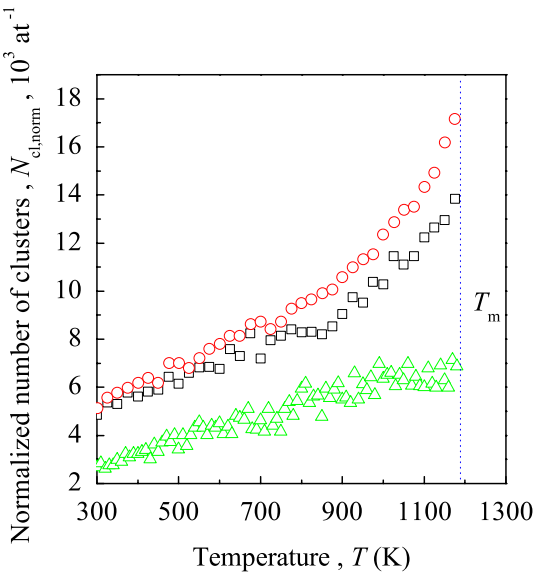


**Fig. 14** The normalized number $N_{cl,norm}$ of clusters of defective atoms as a function of the temperature $T$. The equilibrium melting point $T_{m,0}$ is marked by the vertical dotted line. Data pertain to the bulk (○), plane free surface (□) and particle (△) systems

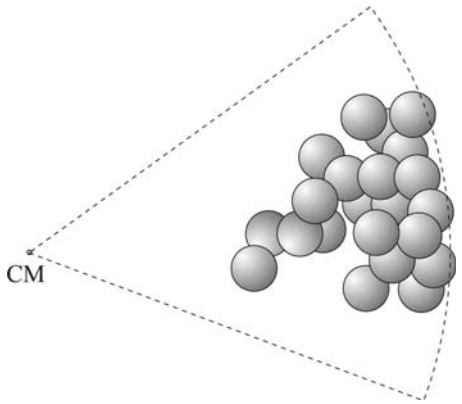


**Fig. 15** A cluster of defective atoms inside the 8 nm particle. The particle shape is schematically reproduced by dotted lines and curve. The particle center of mass is also indicated

interface and is characterized by filamentary structures extending into the particle bulk. The clusters possess then a shape similar to the one already observed in the case of the heterogeneous melting at a plane interface. The formation of clusters with filamentary structures below the solid–liquid interface should be therefore regarded as characteristic of heterogeneous melting.

In analogy with the previous cases, dislocation loops as well as open dislocations with a (111) glide plane are observed together with small hcp crystalline domains. The fraction $\alpha_{def,s}$ of defective atoms involved in lattice defects in each shell s at melting amounts roughly to 0.21 ± 0.02.

## Heterogeneous melting of nanometer-sized cubic particles

The melting process of unsupported cubic particles is very similar to the one displayed by spherical particles. For this reason, results will be only briefly described according to a similar scheme.

Cubic particles with side length of about 4 and 8 nm and (100) plane surfaces were prepared by selecting out from the parent configuration two cubic portions and gradually canceling the interactions between the atoms within the cubes and the ones outside. Cancellation was performed according to the previously described procedure. Relaxed cubes containing 5,708 and 45,629 atoms were obtained. Simulations were carried out within the (*NhT*) statistical ensemble and the temperature was raised at a nominal rate of 0.25 K ps$^{-1}$.

Atomic positions in the bulk-like particle interior were averaged over 2 ps and used to define the crystallographic directions of the fcc lattice. The comparison between theoretically expected positions and real atomic positions permitted the quantification of structural order by means of the static order parameter $S(\boldsymbol{k})$. To this aim, the 4 and 8 nm cubic particles were divided, respectively, into four and eight cubic shell each about 1 nm thick. The fourth and eighth surface shells undergo pre-melting processes approximately at 1,090 K. This $T_{pm}$ value should be compared with the ones of an free and extended (100) plane surface as well as with the one of a curved surface. It appears that the $T_{pm}$ value of cubic particles is larger than for spherical particles and smaller than for an extended plane surface with the same topology. A systematic study of the phenomenon has not been carried out. The preliminary results suggest nevertheless that the observed

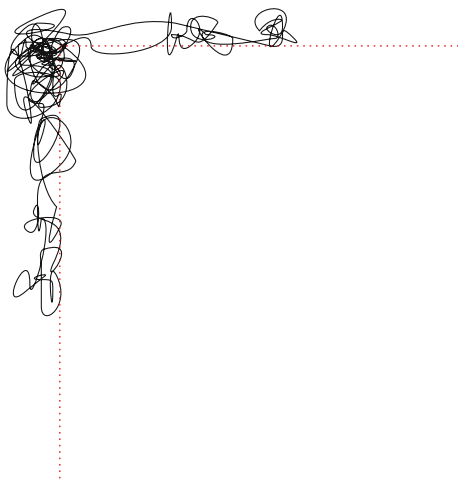

**Fig. 16** The atomic trajectory of an edge atom belonging to a cubic nanometer-sized particle. Edge and free surfaces are indicated by the dotted lines

**Table 3** The pre-melting point $T_{pm}$, the melting point $T_m$ and the latent heat of fusion $\Delta H_m$ for the 4 and 8 nm cubic particles

| | 4 nm | 8 nm |
|---|---|---|
| $T_{pm}$ (K) | 1,090 | 1,090 |
| $T_m$ (K) | 1,240 | 1,250 |
| $\Delta H_m$ (kJ mol$^{-1}$) | 9.31 | 10.82 |

behavior should be a consequence of the unusual mobility of edge atoms. The pre-melting behavior initiates indeed at significantly lower temperatures. The atomic species located at the edges are characterized by a liquid-like mobility already at temperatures as low as 850 K. Their trajectories, one of which is shown in Fig. 16, indicate that a certain number of edge atoms explores the plane free surface occasionally transforming into adatom.

The 4 and 8 nm cubic particles melt approximately at the temperatures $T_m$ of 1,240 and 1,250 K, respectively. Such temperatures are remarkably higher than the melting points of spherical particles and close to the equilibrium melting point $T_{m,0}$ of a system with a free plane surface. The thermal properties of the cubic particles are summarized in Table 3.

The cross-sectional profiles of the fraction $\alpha_{d,s}$ of defective atoms in the various shells at the melting point $T_m$ are similar to the ones already observed in systems with a free surface, i.e. $\alpha_{d,s}$ values decreases smoothly with the distance from the free surface. The fractions $\alpha_{d,3}$ and $\alpha_{d,7}$ of defective atoms in the third and seventh cubic shells are approximately equal to 0.38 and a given cubic shell s undergoing melting is characterized by $\alpha_{d,s}$ values on the order of 0.38 ± 0.02.

The normalized number $N_{cl,norm}$ of defective atom clusters changes with the temperature $T$ as in the case of the 4 nm particle. Both qualitative trend and quantitative features are very similar and will not be reported here for sake of brevity. Of course, once more the behavior can be rationalized by invoking the occurrence of cluster coalescence events. The observed clusters have a shape similar to the one of clusters involved in the heterogeneous melting at a plane interface. Dislocation loops and open dislocations can be again identified as well as small hcp domains. The fraction $\alpha_{def,s}$ of defective atoms involved in lattice defects within each cubic shell s at melting is equal to about 0.22 ± 0.01.

## Heterogeneous melting of a nanometer-sized cylindrical wire

A nanometer-sized Cu wire with circular cross section and radius of about 4 nm was prepared by selecting out from the parent configuration a cylindrical portion and gradually canceling the interactions between the atoms within the wire and the ones outside. Cancellation was performed according to the previously described procedure. A relaxed wire containing 84,221 atoms was obtained. As in the previous cases, simulations were carried out within the ($NhT$) statistical ensemble. Heating was performed at a nominal rate of 0.25 K ps$^{-1}$.

The structural order was quantified by means of the static order parameter $S(\boldsymbol{k})$ taking advantage of atomic positions averaged over 2 ps as previously described. The interior of the cylindrical wire was divided into four cylindrical shell about 1 nm thick. The fourth shell display a pre-melting behavior approximately at 1,070 K. Pre-melting therefore takes place at a temperature $T_{pm}$ comparable with the one displayed by the 4 nm spherical particle. It is also similar to the one of cubic particles. It should be however remembered that in this case the pre-melting behavior of surface atoms is strongly influenced by the mobility of edge atoms. The wire melts approximately at 1,200 K, i.e. at a temperature close to the one of the 4 nm spherical particle. This suggests of course that the melting process is somewhat governed by the free surface

**Table 4** The pre-melting point $T_{pm}$, the melting point $T_m$ and the latent heat of fusion $\Delta H_m$ for the nanometer-sized cylindrical wire

| | |
|---|---|
| $T_{pm}$ (K) | 1,070 |
| $T_m$ (K) | 1,200 |
| $\Delta H_m$ (kJ mol$^{-1}$) | 9.92 |

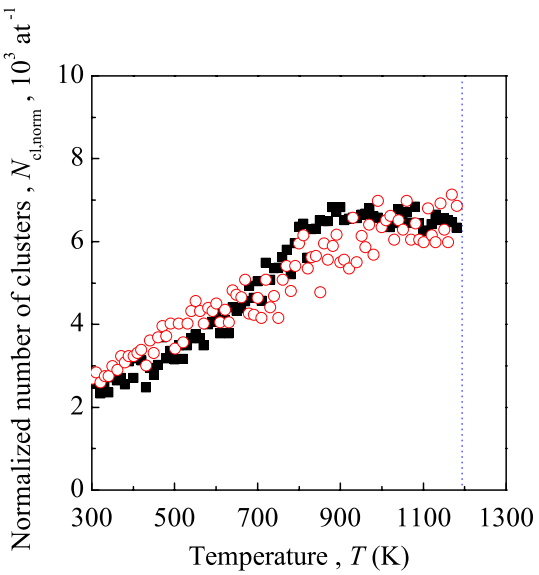


**Fig. 17** The normalized number $N_{cl,norm}$ of clusters of defective atoms as a function of the temperature $T$. The melting point $T_m$ is marked by the vertical dotted line. Data pertain to the nanowire (■) and to the particle (○) systems

curvature. The thermal properties of the cylindrical wire are quoted in Table 4.

As observed in previous cases, the fraction $\alpha_{d,s}$ of defective atoms in the cylindrical shells at the melting point $T_m$ regularly decreases as the distance from the free surface increases. The fraction $\alpha_{d,3}$ of defective atoms in the third cylindrical shell is approximately equal to 0.39. On the average, the cylindrical shells s melt when $\alpha_{d,s}$ is equal to 0.39 ± 0.02.

The normalized number $N_{cl,norm}$ of defective atom clusters is reported in Fig. 17 as a function of the temperature $T$. The $N_{cl,norm}$ values are quite similar to the ones pertaining to spherical particles. However, in the present case the change of slope is considerably more marked and occurs at lower temperatures. It almost defines a maximum, thus indicating that cluster coalescence events are more pronounced than in previous cases. Actually, even though the arrangement of defective atoms in the clusters is similar to the one already observed when a free surface is present, the number of defective atoms in a single cluster can become as large as 8,000. A cluster extending along the z Cartesian direction for about 5 nm, reported in Fig. 18, was also observed. The fraction $\alpha_{def,s}$ of defective atoms involved within each cubic shell s at melting in identified lattice defects such as dislocation loops and lines is equal to about 0.23 ± 0.01.

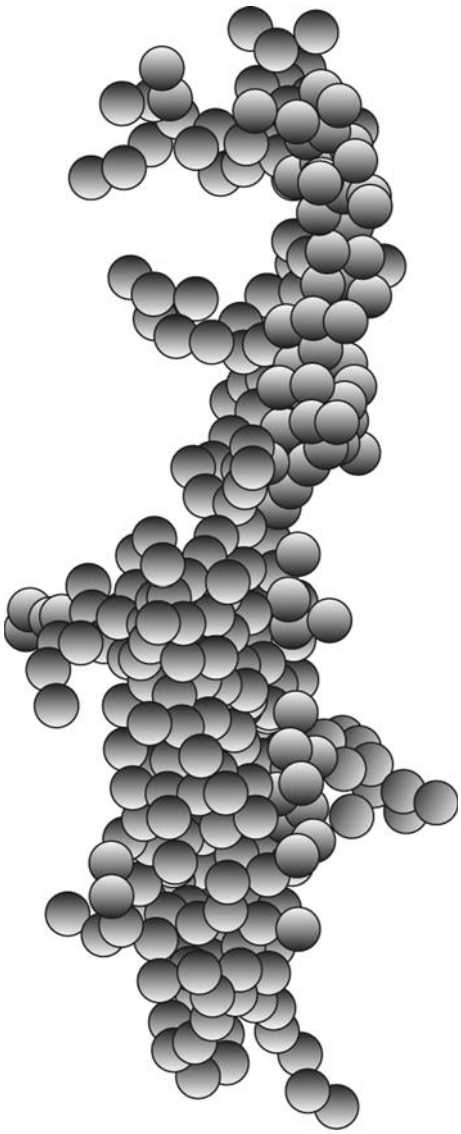

**Fig. 18** A cluster of defective atoms extending along the nanowire axis

## Conclusions

The present study analyzed the mechanism of homogeneous and heterogeneous melting processes. Homogeneous melting takes place in a surface-free perfect bulk system at the first limit of superheating $T_m^k$. The formation of atoms with defective coordination seems to play a key role in the failure of the crystalline lattice. They form relative large aggregates the number and size of which vary with the temperature. The heterogeneous melting process was studied in a semi-crystal bulk system, in unsupported nanometer-sized spherical and cubic particles and finally in a nanometer-sized cylindrical wire. These systems have the common feature of possessing either plane or curve free surfaces of different extension. In heterogeneous solid–liquid transition, the surface must be regarded as a preferential nucleation site. As a consequence, surface layers undergo pre-melting phenomena mostly as a result of the proliferation of vacancies. Successively, the solid–liquid interface propagates at rates dependent on the temperature to the entire system. Propagation is intimately related to the formation of a critical amount of defective atoms, or alternatively of lattice defects. In all the cases, including homogeneous melting, the phase transition of a given volume of solid occurs when the fraction of defective atoms it contains is roughly equal to 0.39. At melting, the fraction of defective atoms involved in the formation of lattice defects is also approximately equal for all the systems investigated, amounting on the average to 0.2. These regularities not only suggest the existence of an intimate connection between homogeneous and heterogeneous melting processes, but also support mechanistic scenarios for the solid–liquid phase transformation laying emphasis on the role of topological defects such as dislocations. Systematic investigations on different systems must be considered as necessary to further explore the mechanistic details of these processes.

**Acknowledgements** Dr. L. Burakovsky, Theoretical Division, Los Alamos National Laboratory, U.S.A., and Prof. G. Cocco, Department

of Chemistry, University of Sassari, Italy, are gratefully acknowledged for stimulating discussions and useful suggestions. A. Ermini, ExtraInformatica s.r.l., is gratefully acknowledged for his kind assistance. Financial support was given by the University of Cagliari.

## References

1. Moriarty P (2001) Rep Prog Phys 64:297
2. Jortner J, Rao CNR (2002) Pure Appl Chem 74:1491
3. Hill TL (2001) Nano Lett 1:273
4. Alivisatos P (1996) Science 271:933
5. Pawlow P (1909) Z Phys Chem (Munich) 65:1
6. Hollomon TH, Turnbull D (1953) Prog Metal Phys 4:333
7. Takagi M (1954) J Phys Soc Jpn 9:359
8. Wronski CRM (1967) Br J Appl Phys 18:1731
9. Coombes CJ (1972) J Phys F: Metal Phys 2:441
10. Hanszen K-J (1960) Z Phys 157:523
11. Buffat PH, Borel J-P (1976) Phys Rev A 13:2287
12. Couchman PR, Jesser WA (1977) Nature 269:481
13. Reiss H, Mirabel P, Whetten RL (1988) J Phys Chem 92:7241
14. Sakai H (1996) Surf Sci 351:285
15. Peters KF, Cohen JB, Chung Y-W (1998) Phys Rev B 57:13430
16. Lai SL, Guo JY, Petrova V, Ramanath G, Allen LH (1996) Phys Rev Lett 77:99
17. Yu Efremov M, Schiettekatte F, Zhang M, Olson EA, Kwan AT, Berry LS, Allen LH (2000) Phys Rev Lett 85:3560
18. Zhang M, Yu Efremov M, Schiettekatte F, Olson EA, Kwan AT, Lai SL, Greene JE, Allen LH (2000) Phys Rev B 62:10548
19. Olson EA, Yu Efremov M, Zhang M, Zhang Z, Allen LH (2005) J Appl Phys 97:034304
20. Dash JG (2002) Contemp Phys 43:427
21. Stillinger FH, Weber TA (1984) Science 228:983
22. Kleinert H (1989) Gauge theory in condensed matter. World Scientific, Singapore
23. Tallon JL (1989) Nature 342:658
24. Lu K, Li Y (1998) Phys Rev Lett 80:4474
25. Cahn RW (2001) Nature 413:582
26. Jin ZH, Gumbsch P, Lu K, Ma E (2001) Phys Rev Lett 87:055703
27. Lindemann FA (1910) Phys Z 11:609
28. Gilvarry JJ (1956) Phys Rev 102:308
29. Born M, Huang K (1954) Dynamical theory of crystal lattices. Clarendon Press, Oxford
30. Kosterlitz J, Thouless DJ (1973) J Phys C 6:1181
31. Nelson DR, Halperin BI (1979) Phys Rev B 19:2457
32. Young AP (1979) Phys Rev B 19:1855
33. Burakovsky L, Preston D, Silbar R (2000) Phys Rev B 61:15011
34. Gomez L, Dobry A, Geuting Ch, Diep HT, Burakovsky L (2003) Phys Rev Lett 90:095701
35. Gomez L, Gazza C, Dacharry H, Penaranda L, Dobry A (2005) Phys Rev B 71:134106
36. Broughton JQ, Gilmer GH (1986) Phys Rev Lett 56:2692
37. Rosato V, Ciccotti G, Pontikis V (1986) Phys Rev B 33:1860
38. Honeycutt JD, Andersen HC (1987) J Phys Chem 91:4950
39. Phillpot SR, Lutsko JF, Wolf D, Yip S (1989) Phys Rev B 40:2831
40. Lutsko JF, Wolf D, Phillpot SR, Yip S (1989) Phys Rev B 40:2841
41. Hall BD, Flueli M, Monot R, Borel J-P (1991) Phys Rev B 43:3906
42. Cleveland CL, Luedtke WD, Landman U (1999) Phys Rev B 60:5065
43. Qi Y, Ĉağin T, Johnson WL, Goddard WA III (2001) J Chem Phys 115:385
44. Delogu F (2005) Phys Rev B 72:205418
45. Ducastelle F (1970) J Phys (Paris) 31:1055
46. Rosato V, Guillope M, Legrand B (1989) Phil Mag A 59:321
47. Cleri F, Rosato V (1993) Phys Rev B 48:22
48. Wollenberger HJ (1996) In: Cahn RW, Haasen P (eds) Physical metallurgy, 4th edn. Amsterdam, North Holland
49. Brandes EA, Brook GB (eds) (1992) Smithells metals reference handbook, 7th edn. Butterworth-Heinemann, Oxford
50. Finnis MW, Sinclair JF (1984) Phil Mag A 50:45
51. Daw MS, Baskes MI (1984) Phys Rev B 29:6443
52. Andersen HC (1980) J Chem Phys 72:2384
53. Nose' S (1984) J Chem Phys 81:511
54. Parrinello M, Rahman A (1981) J Appl Phys 52:7182
55. Allen MP, Tildesley D (1987) Computer simulation of liquids. Clarendon Press, Oxford
56. Li J, Van Vliet KJ, Zhu T, Yip S, Suresh S (2002) Nature 418:307
57. Belonoshko A, Skorodumova NV, Rosengren A, Johansson B (2006) Phys Rev B 73:012201
58. Somer FL Jr, Canright GS, Kaplan T (1998) Phys Rev E 58:5748
59. Quinn RA, Goree J (2001) Phys Rev E 64:051404
60. Tartaglino U, Zykova-Timan T, Ercolessi F, Tosatti E (2005) Phys Rep 411:291
61. Zheng XH, Grieve R (2006) Phys Rev B 73:064205
62. Delogu F (2005) J Phys Chem B 109:15291
63. Delogu F (2006) J Phys Chem B 110:3281